International Journal of Earth Sciences (2024) 113:539–554
https://doi.org/10.1007/s00531-023-02375-6

ORIGINAL PAPER

Petrogenesis of Late Devonian felsic volcanic rocks of Avalonia from Burin Peninsula, Newfoundland: relation to A-type granites and fluorite mineralization

Jaroslav Dostal[1] · **Luigi Solari**[2] · **Changqian Ma**[3]

Received: 25 August 2023 / Accepted: 2 December 2023 / Published online: 8 February 2024

Abstract
Late Devonian felsic volcanic rocks of the Grand Beach complex (GBC) of Avalonia from the Burin Peninsula, southeastern Newfoundland (northwestern Appalachians) are part of an overstep sequence overlying the Neoproterozoic basement. The volcanic complex is composed of volcanic and volcaniclastic rocks deposited in a post-tectonic extensional setting proximal to the St. Lawrence granite (SLG), a Devonian pluton associated with a prominent vein-type fluorite mineralization. The volcanic rocks are alkali rhyolites, which are weakly peraluminous and exhibit geochemical characteristics of A-type felsic magmas, such as low FeO_t, MgO, CaO, and TiO_2 but high contents of alkalis, Nb, Y, and Zr and high Ga/Al and FeO_t/MgO ratios. They have positive $\varepsilon_{Nd}(t)$ values (~ + 2.5) and their Nd-depleted mantle model ages (~ 0.9 Ga) are consistent with derivation of the parental magma from metasomatized dry Avalonian lower crustal basement via partial melting followed by fractional crystallization. The U–Pb zircon age for the volcanic complex (375.6 ± 1.1 Ma) is closely comparable to the age of the SLG, suggesting that they were emplaced during the same magmatic episode. They also have similar chemical and isotopic compositions, suggesting that the GBC represents a volcanic equivalent of the SLG. The compositional differences between the volcanic rocks and the main phase of the granite pluton, including higher oxidation state of the GBC, reflect the interaction of the parental magma with crustal material and fluids. The close proximity of SLG and GBC suggests that the volcanic complex could host fluorite mineralization.

Keywords Granite · Rhyolite · Devon · Avalonia · Newfoundland · Fluorite mineralization

Introduction

Understanding the relationship between the highly evolved plutonic and volcanic systems is essential to the knowledge of the evolution of highly silicic magma systems. These systems play an important role in discussions of the growth of continents, continental crust evolution through time, and the formation of highly evolved magma associated with various rare metal mineralization (e.g., Annen et al. 2015; Lundstrom and Glazner 2016). These links also allow relating magmatic activity in modern volcanic settings to exposures of the plutonic roots of ancient magmatic belts. During such an investigation, basic questions are—how do plutons and volcanic rocks relate petrogenetically? Did the same processes form them, or did they arise from different processes (e.g., Bachmann et al. 2007; Cheng et al. 2018)? Do spatially and temporally related volcanic and plutonic rocks have similar major- and trace-element characteristics and similar ranges in isotopic ratios?

To evaluate the possible genetic link between approximately coeval Paleozoic volcanic and plutonic rocks associated with fluorite mineralization, we investigated the Devonian volcanic rocks from southeastern Newfoundland (Grand Beach complex, GBC hereafter) and their potential relation to the St. Lawrence Granite (SLG), which hosts a significant deposit of fluorite.

✉ Jaroslav Dostal
jarda.dostal@smu.ca

[1] Department of Geology, Saint Mary's University, 923 Robie Street, Halifax, NS B3H 3C3, Canada

[2] Centro de Geosciencias, Universidad Nacional Autonoma de Mexico, Campus Juriquilla, 76230 Queretaro, Qro, Mexico

[3] State Key Laboratory of Geological Processes and Mineral Resources, China University of Geosciences, Wuhan 430074, China

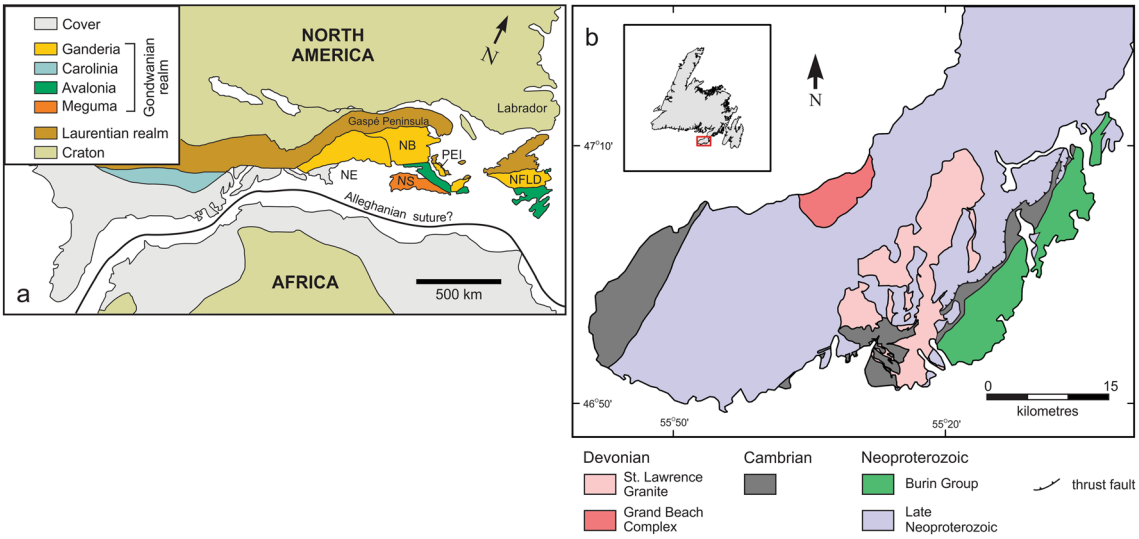

Fig. 1 **a** Map showing the major lithotectonic units of the northern Appalachian orogenic belt (modified after Williams 1984; Hibbard et al. 2006; van Staal et al. 2009). *NE* New England, *NB* New Brunswick, *NS* Nova Scotia, *PEI* Prince Edward Island, *NFLD* Newfoundland. **b** Geologic map of southern part of the Burin Peninsula (southern Newfoundland) showing St. Lawrence Granite and Grand Beach Complex (modified from Magyarosi 2022). The inset in the upper left is a sketch map of Newfoundland depicting the location of Burin Peninsula

Geologic background

The GBC is located in the Avalon terrane (Avalonia) of the Northern Appalachians (Fig. 1a), which is extended along the eastern margin of North America from eastern Newfoundland through Nova Scotia and Maine to northern Georgia. In Newfoundland, Avalonia, the easternmost composite terrane of the Northern Appalachians is bounded by the Dover Fault in the west and the Grand Banks in the east.

Avalonia (an exotic peri-Gondwanan terrane or suspect crustal block) was accreted to the composite Laurentia (North American craton) during the Late Silurian (e.g., van Staal et al. 2009). The terrane is composed of fault-bounded Neoproterozoic volcano-sedimentary belts, which were affected by the Neoproterozoic Avalonian orogeny (low-grade metamorphism only) and subsequently overlain by Cambrian–lower Ordovician platformal strata (O'Brien et al. 1996; Mills et al. 2021). The Avalon terrane was intruded by numerous Neoproterozoic plutons and several Paleozoic granitic intrusions.

The GBC lies in the southern part of the Burin Peninsula of southwestern Newfoundland (Fig. 1b). In this area, the peninsula is dominated by the Neoproterozoic Marystown Group (590–575 Ma), a bimodal sequence of volcanic and volcanoclastic rocks with minor clastic sediments and by the SLG, a Devonian granitic pluton associated with a prominent vein-type fluorite mineralization.

The GBC is a Devonian sequence of felsic volcanic and volcaniclastic rocks and associated comagmatic quartz porphyries overlying Neoproterozoic rocks along Fortune Bay (O'Brien et al. 1977; Strong et al. 1978). The complex is about 12 km long with a width up to about 5 km. It underlies an area of about 40 km^2. The volcanic rocks have a thickness of about 200 m (O'Brien et al. 1977).

The SLG is an elongated (NE–SW trending) pluton, about 35 km long and up to ~ 15 km wide (Fig. 1b). It superimposed a distinct contact metamorphic aureole on the country rocks, has generally sharp external contacts, and appears to be emplaced along north–south extensional faults (e.g., Kerr et al. 1993a). The SLG hosts over 40 significant fluorite-bearing veins, varying in width from a few centimeters to locally over 30 m with a strike length ranging up to 3 km. These veins occur in faults and are composed of several phases/generations of fluorite. Their textures indicate the epithermal character of the deposit (Magyarosi 2022). The deposit is estimated to contain about 22 Mt of fluorite (Magyarosi 2022). Several studies postulated that there is a genetic relationship between granites and related rocks and the fluorite deposit (e.g., Teng and Strong 1976; Strong et al. 1984; Kerr et al. 1993a; Magyarosi 2022; Magyarosi et al. 2019).

The age of the GBC is poorly known. It was considered to belong to the Late Precambrian volcanic suite of the Marystown Group (Strong et al. 1978; Krogh et al. 1988). Alternatively, Strong et al. (1978) suggested that the complex could be related to the nearby SLG. Krogh et al. (1988) obtained a U–Pb zircon age of 394 + 6/–4 Ma for the GBC,

Table 1 Whole-rock analyses of the volcanic rocks of the GBC

(a) Wt.%	73–1	73–2	73–3	73–4	73–5	73–6	73–7	74–1	74–2	74–3
SiO_2	77.15	77.06	77.64	77.71	77.03	77.96	77.23	77.06	77.47	78.09
TiO_2	0.09	0.11	0.08	0.08	0.07	0.09	0.08	0.08	0.08	0.08
Al_2O_3	11.79	11.67	11.72	11.62	11.80	11.80	11.74	11.76	11.75	11.75
$Fe_2O_3^t$	1.36	1.42	1.37	1.28	1.21	1.19	1.31	1.34	1.29	1.32
MnO	0.02	0.02	0.02	0.02	0.02	0.02	0.02	0.02	0.02	0.02
MgO	0.17	0.20	0.17	0.17	0.17	0.16	0.15	0.13	0.16	0.14
CaO	0.36	0.51	0.34	0.33	0.28	0.23	0.33	0.28	0.33	0.33
Na_2O	3.59	3.62	3.59	3.43	3.30	3.49	3.54	3.46	3.52	3.65
K_2O	4.64	4.72	4.80	4.96	5.13	4.87	4.86	5.01	4.81	4.71
P_2O_5	0.01	0.02	0.01	0.01	0.01	0.01	0.01	0.01	0.01	0.01
LOI	0.29	0.41	0.28	0.31	0.30	0.30	0.27	0.29	0.30	0.26
Total	99.47	99.74	100.02	99.91	99.31	100.11	99.53	99.44	99.74	100.37
ppm										
Li	20.4	22.3	20.3	17.8	17.8	17.9	19.1	20.9	21.4	20.1
Co	0.7	0.8	0.71	0.47	0.48	0.63	0.45	0.56	0.52	0.54
Ni	2.55	2.53	3.01	2.15	2.33	2.64	2.19	3.08	2.09	2.49
V	3.60	4.65	3.69	3.11	3.94	5.98	2.89	2.86	3.59	2.85
Ga	22.8	22.3	21.9	22.0	22.3	20.5	21.8	21.5	21.8	21.0
Rb	203	198	203	218	228	209	211	212	208	200
Sr	32.4	33.4	35.1	43.5	40.2	44.3	34.3	29.7	30.6	32.0
Y	63.1	64.1	64.6	74.5	70.9	54.5	69	70.6	65.5	59.4
Zr	144	146	154	172	149	142	147	149	149	148
Nb	40.9	41.7	43.1	41.6	40.7	42.2	42.3	41.5	43.1	41.4
Sn	5.96	6.43	6.30	6.06	6.32	5.98	6.09	5.95	5.98	5.65
Cs	2.25	2.24	2.22	3.09	2.73	2.38	2.57	2.31	2.39	2.28
Ba	65.2	60.6	65.3	58.9	65.7	70.1	59.0	65.1	60.7	62.6
La	42.4	42.9	40.2	38.3	45.0	35.3	41.7	43.6	38.2	36.7
Ce	88.2	89.9	88.6	85.8	91.2	75.0	88.0	84.0	84.9	81.8
Pr	10.8	11.1	10.7	10.3	11.6	9.17	10.9	11.1	10.0	9.54
Nd	41.9	42.9	40.2	39.8	45.5	35.3	42.4	44.2	39.6	36.6
Sm	10.1	10.2	9.84	10.4	10.8	8.67	10.8	10.8	10.5	9.23
Eu	0.15	0.19	0.15	0.14	0.18	0.18	0.17	0.18	0.16	0.13
Gd	9.67	10.1	9.39	9.97	11.0	8.52	10.4	10.6	9.75	8.99
Tb	1.77	1.84	1.84	1.89	2.00	1.62	1.97	1.95	1.83	1.69
Dy	11.1	11.4	11.3	12.3	12.2	10.1	11.8	12.2	11.4	10.6
Ho	2.16	2.24	2.19	2.53	2.45	2.06	2.40	2.44	2.38	2.04
Er	5.98	6.10	6.17	6.82	6.63	5.67	6.56	6.79	6.33	5.57
Tm	0.96	0.94	1.01	1.04	0.96	0.84	0.96	1.02	0.96	0.87
Yb	6.14	6.21	6.34	6.91	6.60	5.84	6.69	6.67	6.46	5.76
Lu	0.86	0.9	0.89	0.97	0.89	0.81	0.91	0.95	0.91	0.85
Hf	6.37	6.04	6.61	6.90	6.31	5.95	6.07	5.97	6.11	5.99
Ta	3.00	2.99	3.14	3.05	2.99	3.07	3.14	3.09	3.15	3.00
Pb	12.7	12.5	8.35	6.93	8.71	7.73	9.71	8.21	10.1	10.1
Th	20.7	21.2	21.3	20.6	21.1	21.4	21.7	21.4	21.2	20.5
U	4.58	4.57	4.26	4.36	4.30	4.76	5.11	4.39	4.91	4.35

Table 1 (continued)

(b) Wt.%	86–2	87–1	87–2	87–3	88	66–2	66–3	66–4	24	25
SiO_2	70.08	77.55	77.46	77.29	77.15	77.82	77.92	77.51	75.44	76.50
TiO_2	0.40	0.08	0.09	0.09	0.09	0.09	0.08	0.09	0.23	0.22
Al_2O_3	14.01	11.68	11.60	11.57	12.12	11.89	11.88	11.80	10.51	10.70
$Fe_2O_3^t$	4.14	1.43	1.78	1.75	1.75	1.16	1.12	1.32	3.69	3.60
MnO	0.10	0.02	0.02	0.02	0.02	0.02	0.01	0.02	0.10	0.12
MgO	0.87	0.16	0.24	0.23	0.18	0.16	0.19	0.22	0.13	0.15
CaO	1.63	0.15	0.14	0.15	0.14	0.15	0.17	0.16	0.28	0.16
Na_2O	3.32	3.36	3.04	3.09	3.32	3.63	3.55	3.55	2.91	2.99
K_2O	2.86	5.22	5.47	5.39	4.98	4.86	4.76	4.84	5.77	5.45
P_2O_5	0.08	0.01	0.01	0.01	0.02	0.01	0.02	0.01	0.01	0.01
LOI	2.73	0.30	0.37	0.37	0.42	0.25	0.39	0.29	0.35	0.24
Total	100.21	99.97	100.21	99.96	100.19	100.03	100.09	99.80	99.40	100.14
ppm										
Li	6.20	5.65	6.03	6.47	4.93	12.8	12.9	14.7	55.8	53.4
V	28.0	4.53	5.95	4.12	4.77	4.52	4.15	5.21	1.78	2.51
Co	4.81	0.55	1.01	0.86	0.58	0.51	0.61	0.62	0.28	0.22
Ni	5.22	2.18	3.23	2.66	1.90	1.70	2.43	2.92	2.55	1.83
Ga	17.1	18.0	18.4	17.8	19.6	21.0	21.4	21.9	30.4	31.0
Rb	109	194	198	204	174	190	188	196	275	267
Sr	159	26.3	31.5	30.7	23.8	40.4	32.2	39.2	11.3	12.4
Y	36.0	40.6	80.2	71.0	39.8	53.4	48.3	52.7	102	104
Zr	189	159	164	138	168	149	182	163	812	828
Nb	7.94	39.1	38.7	39.5	35.7	39.4	40.4	41.1	64.1	60.4
Sn	2.03	5.13	5.49	4.99	5.11	5.35	5.67	6.04	7.25	7.05
Cs	6.84	2.77	2.92	2.88	2.52	2.55	2.60	2.54	3.11	3.65
Ba	612	98.2	120	113	96.7	71.2	65.8	69.2	118	168
La	25.3	17.1	62.0	53.2	52.5	30.2	17.1	24.3	88.5	88.5
Ce	50.2	51.8	56.5	51.0	56.0	84.0	39.4	76.1	187	187
Pr	6.34	4.08	15.3	13.1	12.3	7.06	3.46	5.54	22.2	22.5
Nd	27.1	15.7	59.4	51.8	47.3	25.9	11.8	19.9	88.3	91.1
Sm	5.87	3.96	13.5	12.0	10.5	6.39	2.83	5.72	17.5	18.5
Eu	1.43	0.11	0.31	0.25	0.25	0.15	0.11	0.12	0.69	0.66
Gd	5.60	4.37	12.9	12.1	9.58	6.76	3.86	5.87	17.3	17.3
Tb	0.96	0.99	2.21	1.99	1.48	1.44	1.11	1.33	2.97	3.03
Dy	6.01	6.67	12.5	11.4	7.57	9.5	8.14	9.26	18.6	18.8
Ho	1.24	1.52	2.5	2.29	1.42	1.99	1.73	1.95	3.53	3.58
Er	3.50	4.33	6.67	6.08	3.59	5.46	4.94	5.59	10.0	10.3
Tm	0.58	0.72	1.11	0.99	0.58	0.87	0.77	0.85	1.49	1.56
Yb	3.91	4.81	6.38	5.98	3.61	5.93	5.32	5.78	10.6	10.2
Lu	0.67	0.79	0.96	0.97	0.68	0.82	0.75	0.81	1.41	1.5
Hf	5.28	6.35	6.34	5.68	6.2	6.32	6.82	647	20.8	20.9
Ta	0.55	2.95	2.78	2.86	2.57	2.93	2.92	3.05	3.93	3.82
Pb	9.93	11.9	15.2	14.1	9.93	9.75	11.0	9.37	18.6	44.4
Th	7.29	20.5	20.1	20.3	18.9	19.9	20.0	20.2	21.4	21.6
U	1.73	2.10	2.34	2.53	3.02	4.08	3.44	4.46	4.56	5.77

Fresh samples 73–1 to 74–3, *Altered group 1* samples 86, 87 and 88, *Altered group 2* samples 66, *Winterland porphyry (SLG)* 24, 25

but considered to be tentative, because it was based on two discordant fractions. Kerr et al. (1993a) questioned the validity of this age determination. Thus, the age of the GBC is uncertain.

There are several age determinations for the St. Lawrence granite intrusion. Bell et al (1977) reported a whole-rock Rb–Sr isochron age of 344 ± 5 Ma. Subsequently, Kerr et al. (1993a) obtained a U–Pb zircon age of 374 ± 2 Ma, whereas Magyarosi et al. (2019) reported a U–Pb zircon age of 377.2 ± 1.3 Ma from a sill in the central part of the pluton (AGS porphyry). These age determinations are typical of the ages of the widespread Devonian intrusions of the Avalon terrane in Newfoundland (e.g., Kerr et al. 1993a; Kellett et al. 2014).

Analytical methods

Major-elements analyses of whole rocks were done by an X-ray fluorescence spectrometer (Rigaku 3080E1) at the Analytical Institute of the Bureau of Geology and Mineral Resources, Hubei Province (China). Relative standard deviations are within 5%. Trace elements were determined using an Agilent 7700e ICP-MS at the Wuhan SampleSolution Analytical Technology Co., Ltd. (Wuhan, China). The samples were digested by HF and HNO_3 in Teflon bombs. The detailed procedure for ICP-MS analyses and analytical precision and accuracy were described in Liu et al. (2010). Analytical precision (relative standard deviation) estimated from repeated analyses of the standard reference samples is better than 5% for rare-earth elements and 5–12% for other trace elements (Table 1a and b).

The Sr–Nd isotopic compositions of two samples (74–3, 73–6) were determined using a Thermo Triton Plus thermal ionization mass spectrometer at the Institute of Geology of the Czech Academy of Sciences, Prague (Czech Republic) following the methods described by Ackerman et al. (2020). The external reproducibility of the analyses was monitored through the long-term analyses of NIST SRM 987 (Sr) and JNdi-1 (Nd) solutions, which yielded $^{87}Sr/^{86}Sr$ of 0.710249 ± 5 (2σ, n = 44) and $^{143}Nd/^{144}Nd$ of 0.512099 ± 6 (2σ, n = 26), respectively. The third sample (74–1) selected for the isotope determinations was analyzed by isotope dilution at the Atlantic Universities Regional Facility at the Department of Earth Sciences of Memorial University of Newfoundland (St. John's, Newfoundland, Canada). The Nd and Sr isotopic ratios were determined using a multicollector Finnigan MAT 262 thermal ionization mass spectrometer. Replicate analyses of the LaJolla standard determined during the run yielded an average value for $^{143}Nd/^{144}Nd = 0.511849 \pm 9$ (2σ), while replicate runs for the NIST SRM 987 (Sr) standard gave $^{87}Sr/^{86}Sr = 0.710250 \pm 11$ (2σ). Dostal et al. (2021) gave more information on these procedures.

About 1 kg of the quartz porphyry sample selected for U–Pb geochronology was crushed, ground, and the heavy minerals concentrated using standard techniques (e.g., Solari et al. 2007). About 50 zircon crystals were mounted in epoxy resin, polished to expose their internal structure, and targeted for U–Pb analyses. The selected zircons are elongate, prismatic in shape, with well-preserved bipyramidal terminations. The observed elongation ratio is up to 8:1. Cathodoluminescence (CL) imaging was performed to be able to observe internal structures, potential zoning, help in choosing the analysis target, as well as to help in interpreting the U–Pb results.

Isotope measurements were performed by laser ablation ICP-MS at the Laboratorio de Estudios Isotópicos, Centro de Geociencias, Universidad Nacional Autónoma de Mexico, using a Thermo ICap Qc quadrupole mass spectrometer coupled to a Resolution M050, 193 nm excimer laser ablation workstation. A 23 µm spot was employed, with a repetition rate of 5 Hz and a 6 J/cm-2 of fluence, following the analytical procedures described in Solari et al. (2018). The standard zircon 91,500 (1065.4 ± 0.6 Ma, TIMS age, Wiedenberck et al. 1995) was employed as a primary standard, whereas Plešovice standard zircon (337.13 ± 0.37 Ma, TIMS age, Sláma et al. 2008) was employed as a control standard. During the analytical session, the control standard yielded a concordant age of 338.4 ± 1.6 Ma (n = 12, MSWD = 1.02), in agreement with its accepted age. The NIST 610 glass was used as an external standard for the recalculation of trace and REE element concentrations, employing ^{29}Si as an internal standard isotope, and assuming a stoichiometric Si value of 15.323 mol. Data processing was performed offline using Iolite software v. 4.5 (Paton et al. 2010) and the VizualAge data reduction scheme of Petrus and Kamber (2012). No common Pb correction was applied, since the ^{204}Pb signal (non-radiogenic Pb) is disturbed by the isobar ^{204}Hg. Data were exported from Iolite and the concordia diagrams and mean ages were calculated using IsoplotR (Veermesch 2018). The calculated age uncertainties are 2-sigma.

Results

Petrography

Among various volcanic and volcaniclastic rocks of the Grand Beach complex, felsic ash-flows and felsic ash-falls are abundant and composed mainly of fine-grained quartz-feldspathic groundmass. Other rock-types are volcaniclastic breccia, mudflow deposits, conglomerates, and fine-grained red sandstone. Ash flows pass into massive rhyolite

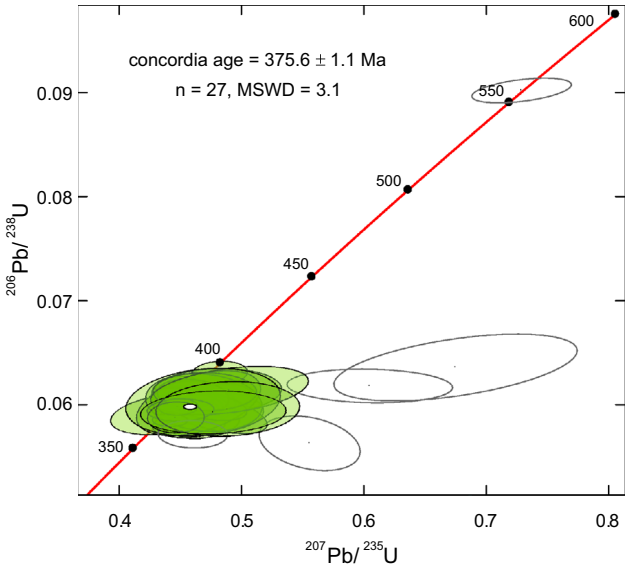

Fig. 2 U–Pb Concordia diagram of the dated sample of the GBC quartz porphyry. Ellipses are plots at 2-sigma uncertainty

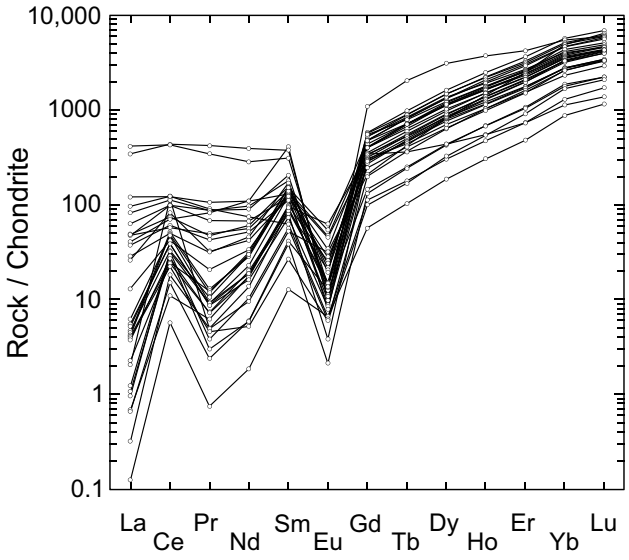

Fig. 3 Chondrite-normalized REE plot of the dated zircon crystals of the GBC quartz porphyry. Normalizing values are after McDonough and Sun (1995)

porphyry and rhyolite flows. Both these rock-types ("quartz porphyry") are porphyritic with phenocrysts of euhedral to embayed quartz, which are 0.1–5 mm in size. Subordinate altered subhedral feldspar phenocrysts sit in a microcrystalline quartz-feldspathic groundmass that is usually altered. The alteration is also manifested by widespread hematization of feldspars and groundmass. The porphyry contains isolated lithic fragments suggesting that they are extrusive (O'Brien et al. 1977). The volcanic and volcaniclastic rocks of the complex contain fragments of rocks, which resemble underlying Neoproterozoic units (O'Brien et al. 1977). Due to poor exposure, it is difficult to recognize the age relationships among the various rock-types.

The SLG rocks are typically medium-grained, equigranular and dominated by quartz and perthitic feldspar with minor mafic minerals-riebeckite–arfvedsonite and aegirine. Accessory minerals include fluorite, calcite, Fe–Ti oxides, zircon, monazite, and apatite. Granites host locally miarolitic cavities and mm- to cm-scale fluorite veinlets. Magyarosi (2022) subdivided the pluton according to geological position into four parts: E- and W-lobes, AGS dikes and sills and Winterland porphyry (along the north margin of the pluton). There are subtle compositional differences among the four parts. The rocks were also modified to varying degrees by several types of alteration (Magyarosi 2022).

U–Pb geochronology

We dated a quartz porphyry of the GBC. Thirty-two out of 35 zircon analyses were considered meaningful, with a discordance of less than 30% (Fig. 2). Of those, five

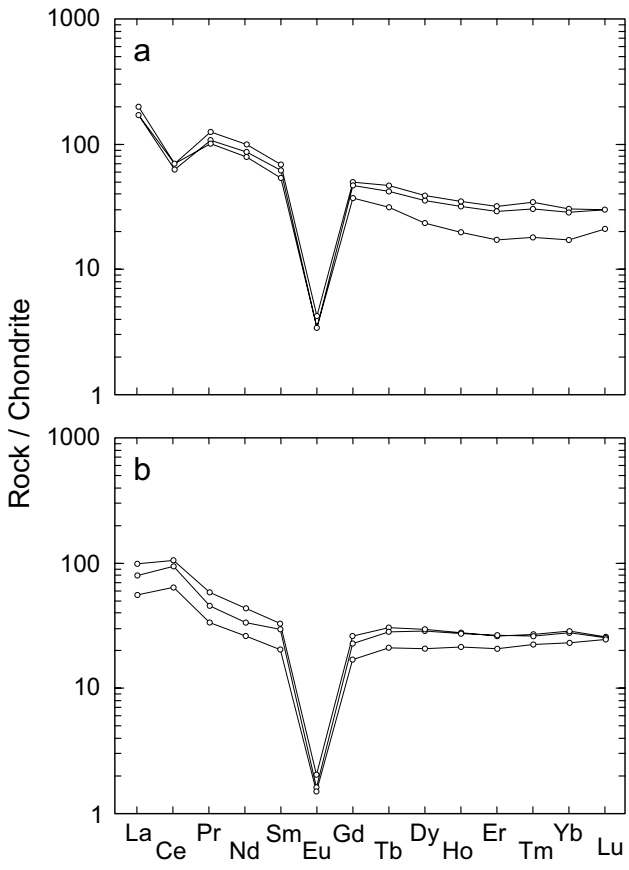

Fig. 4 Chondrite-normalized REE plots of altered GBC rocks: **a** Site 1 (samples 86–2, 87–1, 88); **b** Site 2 (samples 66–2, 66–3, 66–4; Table 1b). Normalizing values after Boynton (1984)

analyses were not considered (uncolored ellipses in Fig. 2). One is inherited (concordant analysis of 556.8 Ma). Three show discordance of 19–23%, probably reflecting a mixing domain. One analysis gave a slightly younger and discordant result ($^{206}Pb/^{238}U$ age of 358.3 Ma, 6% discordant) probably because of Pb loss. The remaining analyses yield a concordant age of 375.6 ± 1.1 Ma that, together with the oscillatory zoning of the zircon growth bands observed under CL, and the REE igneous patterns obtained for the analyzed zircons (Fig. 3) indicate that it represents the crystallization age for the sample. The zircon with an age of ~ 557 Ma is probably inherited from late Neoproterozoic bimodal volcanic rocks, which underlie a large part of the southern Burin Peninsula (O'Brien et al. 1977, 1996; Strong et al. 1978).

Zircon chemistry

The chondrite-normalized REE abundances of the analyzed zircons (Fig. 3) show a depletion of light REE, and an enrichment of heavy REE accompanied by positive Ce and negative Eu anomalies. The patterns are typical of magmatic zircons (e.g., Zhu et al. 2020).

Alteration

The GBC rocks underwent low-grade metamorphism, which replaced glassy groundmass of the porphyries by a fine-grained matrix dominated by various secondary minerals. The secondary processes modified the chemical compositions of some GBC rocks. However, most of the analyzed GBC samples appear to retain their original magmatic composition. In some localities, particularly along the margins of the complex, the rocks show petrographic evidence of alteration. This includes the sericitization and albitization of feldspars and the accumulation of zeolites and calcite in amygdales and fractures. To evaluate the effect of alteration on the rock composition, additional samples were collected from two sites containing distinctly altered samples. The first site is an active quarry along Hwy 210 (Burin Peninsula Hwy) where some samples were overprinted by pervasive hydrothermal alteration (altered group 1, Table 1b). The second site is in the village of Grand Beach where samples were locally modified by fluids containing fluorine as indicated by the presence of traces of fluorite (altered group 2, Table 1b). Alteration affected some trace elements, including the REE. The chondrite-normalized REE plots show differences among the strongly altered samples. Most samples of altered group1 display chondrite-normalized REE patterns with a negative Ce anomaly, while the other altered group 2 has a positive Ce anomaly (Fig. 4).

The irregular chondrite-normalized REE patterns for the altered samples (Fig. 4) indicate non-CHARAC

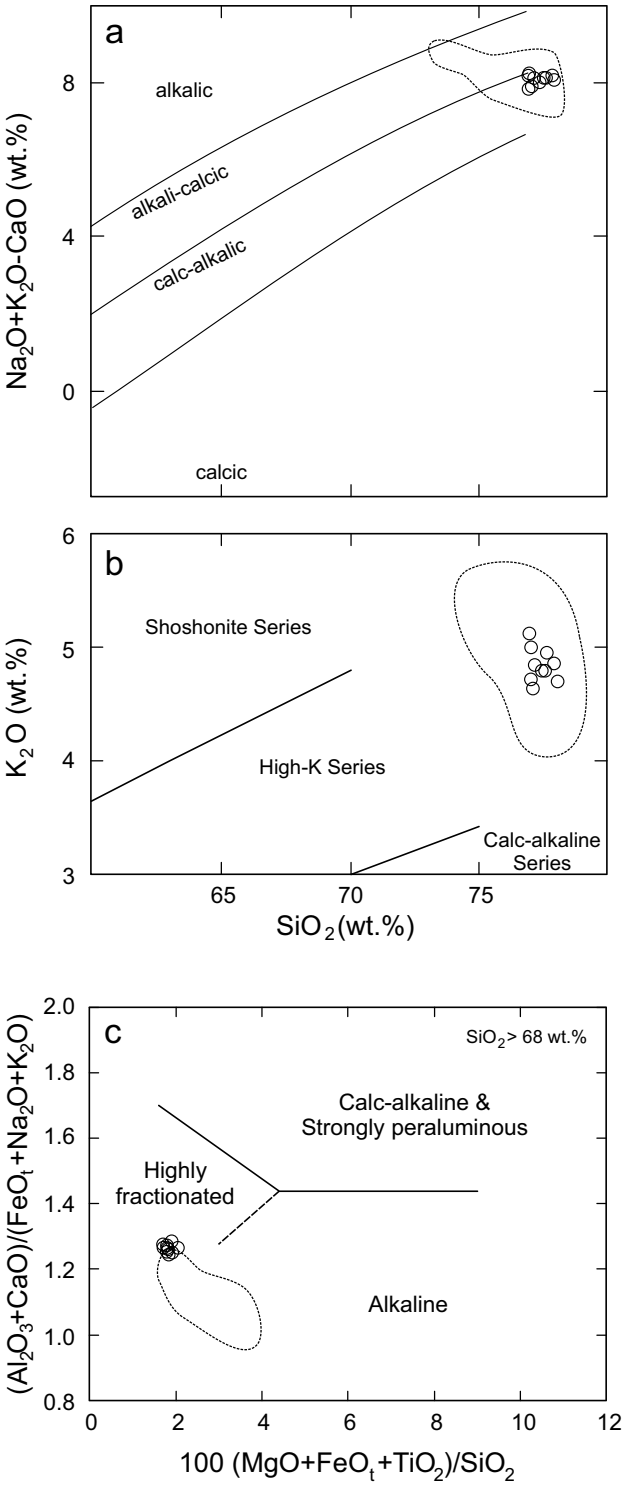

Fig. 5 **a** Classification diagram SiO_2 versus $(Na_2O+K_2O–CaO)$ [MALI] (wt.%) of Frost et al. (2001) for the GBC samples (circles). The dotted curve outlines the field for SLG rocks (data from Magyarosi 2022). **b** SiO_2 versus K_2O (wt.%) diagram discriminating between the calc-alkaline, high-K, and shoshonitic rocks for the samples of the GBC (circles). The dotted curve outlines the field for SLG rocks (data from Magyarosi 2022). **c** Classification diagram of Sylvester (1989) showing the fields of alkaline, calc-alkaline, and highly fractionated granitic rocks for the fresh GBC rocks (circles). The dotted curve outlines the field for SLG rocks (data from Magyarosi 2022)

(CHArge-RAdius Controlled) behavior, i.e., non-magmatic effects (e.g., Bau 1996; Irber 1999; Monecke et al. 2002). Unlike a magmatic CHARAC REE pattern which is characteristically smooth (with the exception of Eu), non-CHARAC patterns likely reflect tetrad effects, which break the lanthanides into four segments of four elements. Enrichment or depletion of various elements results in either convex-up "M-type" or concave-up "W-type" chondrite-normalized REE patterns (e.g., Monecke et al. 2002). Irber (1999) proposed a procedure to quantify the intensity of the tetrad effect. Values of the total tetrad effects larger than unity indicate M-type tetrads, whereas those < 1 indicates W-type. Irber (1999) also argued that the values > 1.1 are significant and clearly visible on the REE plots. The altered rocks of group 1 have the total tetrad values ~ 0.85, while the group 2 has the values ~ 1.2. The tetrad effect was probably inherited from external fluids during or after emplacement of the magma. The fluids were likely modified by alteration of wall rocks (e.g., Monecke et al. 2002). Magyarosi (2022) documented similar alteration processes in the St. Lawrence granite and suggested that the SLG cooled slowly and that the associated hydrothermal activity lagged and lasted longer than the duration of crystallization.

Geochemistry

The quartz porphyries of the GBC have high-silica contents (75–77 wt.% -LOI-free) and relatively uniform major- and trace-element compositions. On the $Na_2O + K_2O$–CaO (MALI)-silica diagram of Frost et al. (2001) (Fig. 5a), the rocks plot in the calc-alkalic field, whereas on the Zr/TiO_2 vs Nb/Y diagram of Pearce (1996) and the multi-element graph of de la Roche et al (1980), they plot in the alkali rhyolite field (Fig. 6). According to the K_2O vs SiO_2 plot (Fig. 5b), the rocks are high K accompanied by K_2O/Na_2O ~ 1.3 to 1.5. The GBC porphyries are weakly peraluminous (Fig. 6) and have high $FeO_t/(FeO_t + MgO)$ ratios (~ 0.9), typical of ferroan granites (Frost et al. 2001). The porphyries have low contents of FeO_t (1–1.6 wt. %), MgO (0.13–0.24 wt. %), CaO (< 0.6 wt.%), and TiO_2 (~ 0.1 wt.%) but high contents of alkalis. According to the classification of Sylvester (1989), the GBC rocks are highly differentiated alkaline granitic/rhyolitic rocks (Fig. 5c). The GBC rocks have trace-element characteristics (Fig. 7) of fractionated A-type post-collision alkali rhyolitic rocks (Harris et al. 1986; Pearce 1996).

The chondrite-normalized REE patterns of the GBC rocks have a distinct light REE (LREE) enrichment accompanied by relatively flat heavy REE (HREE) segments (Fig. 8a) and are characterized by $(La/Yb)_n$ ~ 4 to 5 and $(Gd/Yb)_n$ ~ 1.4. The patterns are generally subparallel and accompanied by negative Eu anomalies. On the primitive mantle-normalized multi-element plots (Fig. 9a), the porphyries are enriched in several large ion lithophile elements (LILE; e.g., Rb) as well as Th and La, but the patterns display negative anomalies for Ba, Sr, P, Eu, Nb, and Ti.

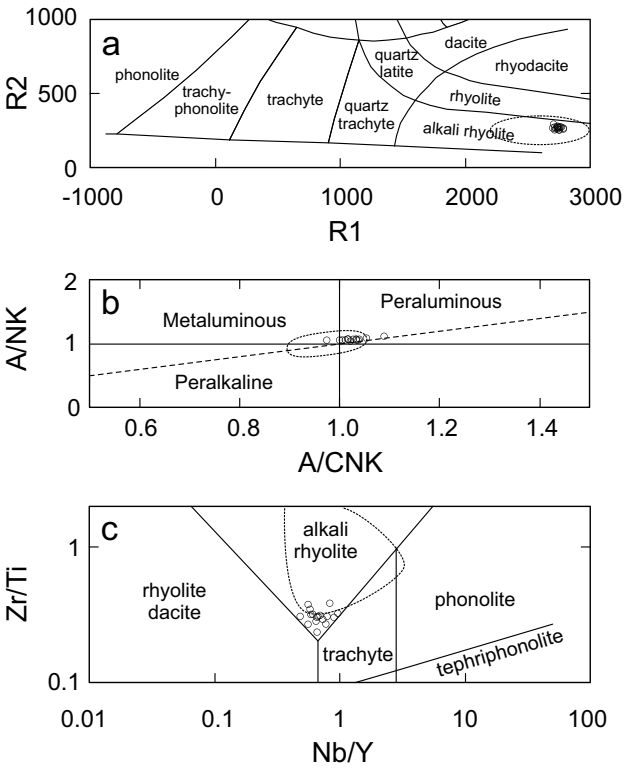

Fig. 6 **a** Multicationic classification plot of De la Roche et al. (1980) [R1: 4Si–11(Na + K)–2(Fe + Ti); R2: 6Ca + 2 Mg + Al] used for the classification of GBC rocks (circles). The dotted curve outlines the field for SLG rocks (data from Magyarosi 2022). **b** Plot of molar $Al_2O_3/(Na_2O + K_2O)$ [A/NK] versus $Al_2O_3/(CaO + Na_2O + K_2O)$ [A/CNK] that discriminates metaluminous, peraluminous, and peralkaline compositions of granitic rocks used for the GBC rocks (circles). The dotted curve outlines the field for SLG rocks (data from Magyarosi 2022). **c** Zr/Ti versus Nb/Y classification diagram of Pearce (1996) for the GBC rocks (circles). The dotted curve outlines the field for SLG rocks (data from Magyarosi 2022)

The $\varepsilon_{Nd}(t)$ values ($t = 377$ Ma; Table 2) for the porphyries fall within a narrow range (~ + 2.5) and are similar to the values reported by Kerr et al. (1995) for SLG and GBC (Table 2). These values are also comparable to the Devonian post-tectonic granitic plutons from the Avalon terrane of Newfoundland (Kerr et al. 1995) and Nova Scotia (Cobequid Highlands, Papoutsa et al. 2016). The Nd-depleted mantle model ages of the porphyries and SLG have a relatively narrow range of ~ 0.9 Ga.

Crystallization temperature and oxygen fugacity conditions

The saturation temperatures of several accessory minerals in felsic magmas can be applied to characterize the origin and thermal history of these felsic rocks. The saturation

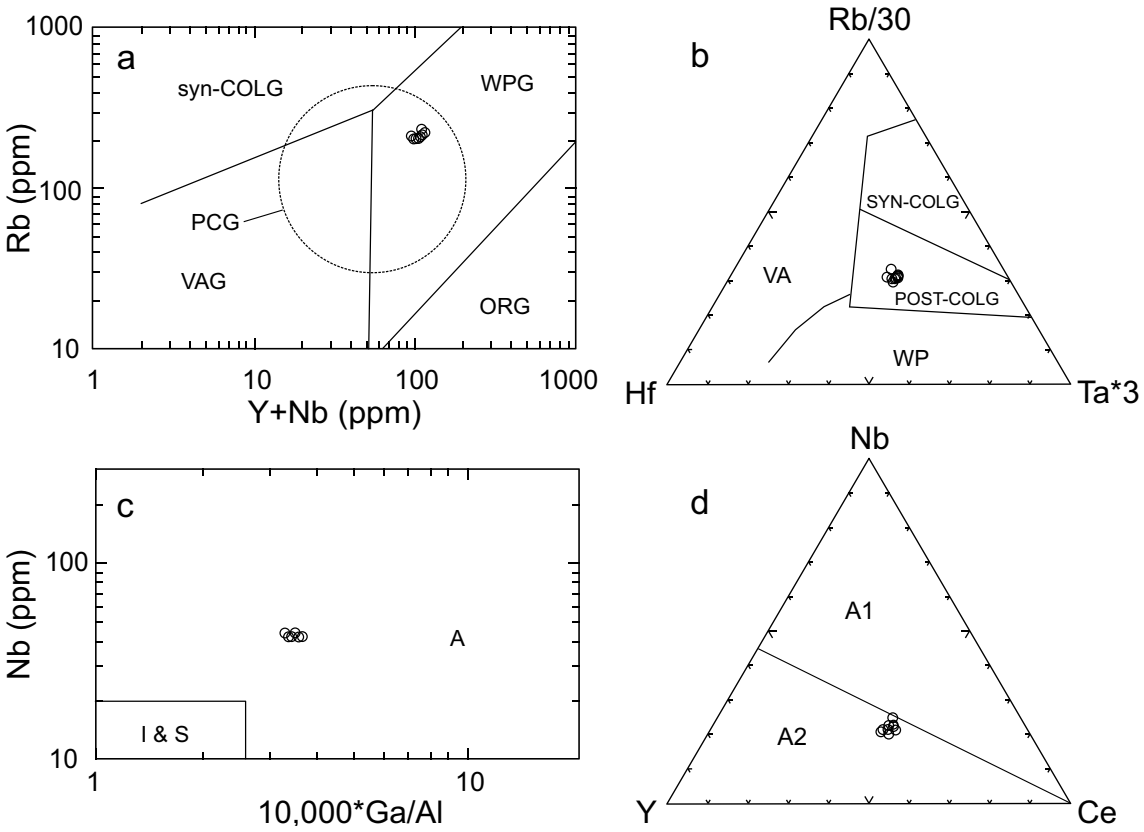

Fig. 7 **a** (Nb + Y) versus Rb (ppm) tectonic discrimination diagram of Pearce (1996) for the fresh GBC rocks. Fields: *ORG* ocean ridge granite, *syn-COLG* syn-collisional granite, *VAG* volcanic-arc granite, *WPG* within-plate granite, *PCG* post-collisional granite. **b** Hf–Rb/30-Ta*3 diagram of Harris et al. (1986) for fresh GBC rocks. Fields: *VA* volcanic-arc granite, *WP* within-plate granite, *SYN-COLG* syn-collisional granite, *POST-COLG* post-collisional granite. **c** (10,000 × Ga/Al) versus Nb (ppm) discrimination diagram of Whalen et al. (1987) for the fresh GBC rocks. Fields: *I&S* I- and S-type granite, *A* A-type granite. **d** Y–Nb–Ce diagram of Eby (1992) for the fresh GBC rocks

temperatures are, in part, related to magma evolution and help assess petrogenetic similarities or differences among the various units of the felsic rocks. In particular, the zircon saturation temperatures (T_{Zr}) were utilized to classify the granites as "hot" (anhydrous with $T_{Zr} > 800$ °C) or "cold" (wet with $T_{Zr} < 800$ °C) (e.g., Miller et al. 2003). Our T_{Zr} results for SLG (E- and W-loops) using the whole-rock analyses of Magyarosi (2022) are well above 800 °C, suggesting that the SLG rocks crystallized from a "hot" and "anhydrous" felsic melt (Table 3). The calculated temperatures for AGS sills (whole-rock data from Magyarosi 2022) and GBC (Table 3) are overlapping but lower relative to the pluton data. We have also calculated the monazite saturation temperatures for these rocks (Table 3). The calculations, which are based on Montel (1993), relate the concentrations of LREE to the bulk composition of the magma. The temperatures are comparable to those obtained for zircon (Table 3). The Ti-in-zircon thermometer ($T_{Ti\text{-}in\text{-}zircon}$; Watson et al. 2006) yielded a zircon temperature of 812 ± 62 °C (Table 3). The value is similar to T_{Zr} for the GBC, indicating that the melt was relatively anhydrous (Li et al. 2018; Wang et al. 2013).

The Ce anomaly of zircon (Fig. 3) can be employed to quantitatively estimate the oxygen fugacity (*f*O2) of the parental magma (Trail et al. 2012). The fO_2 value calculated according to Loucks et al. (2020) indicates nearly neutral conditions for GBC (average of ΔFMQ = – 0.61, where FMQ is the fayalite–magnetite–quartz buffer). The GBC rocks are more oxidized than the SLG rocks, which plot into the field of reduced A-type granites (Fig. 10).

Discussion

Petrogenesis

GBC volcanic rocks are evolved, alkali- and silica-rich rocks with high Fe/Mg and Ga/Al ratios. They are enriched in incompatible trace elements including REE and LILE relative to average granites (Winter 2001) typical of post-orogenic felsic magmatism. The GBC rocks are similar

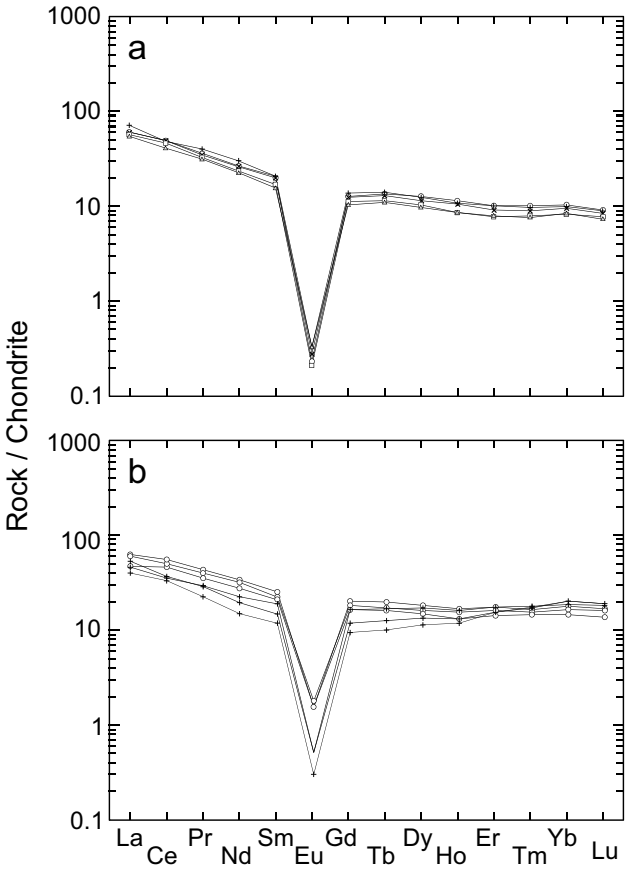

Fig. 8 Chondrite-normalized REE plots of rocks from **a** Grand Beach Complex (Table 1); **b** St. Lawrence Granite (data from Magyarosi 2022). Normalizing values after Boynton (1984)

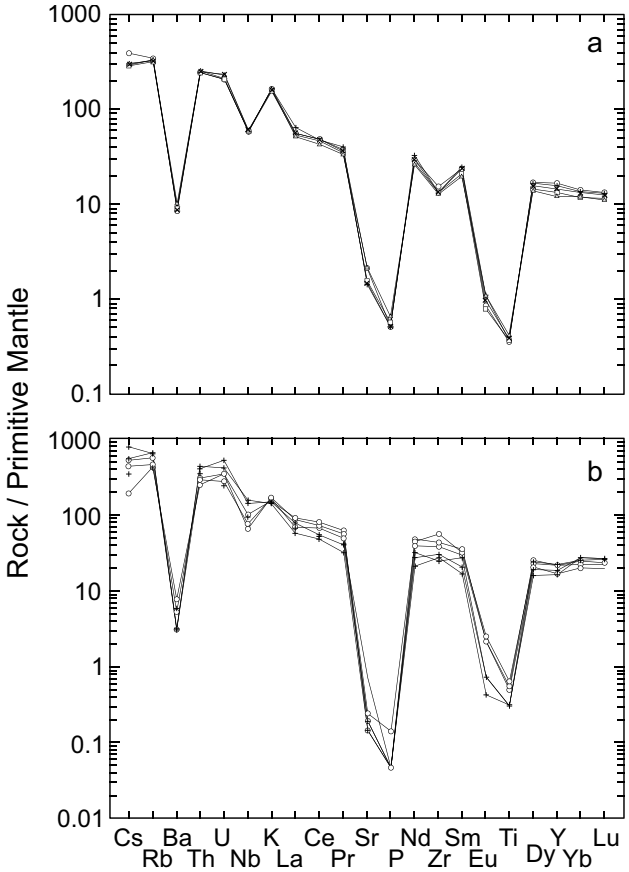

Fig. 9 Primitive mantle-normalized incompatible element abundances of the rocks from **a** Grand Beach Complex and **b** St. Lawrence Granite (data from Magyarosi 2022). Normalizing values after McDonough and Sun (1995). Elements are arranged in the order of decreasing incompatibility from left to right

to several other Devonian granitic rocks from this part of Avalonia in Newfoundland (e.g., Kerr et al. 1993a, b, 1995; Kellett et al. 2014), particularly the SLG rocks, and in the Cobequid Highlands of Nova Scotia (e.g., Papoutsa et al. 2016). According to various classification schemes, they are "A-type" felsic rocks (Fig. 7). A-type granites and volcanic equivalents are thought to be derived from magmas that have an igneous source (Whalen et al. 1987), either by partial melting of rocks or fractional crystallization of mafic magma (Eby 1992; Frost et al. 2001). The low concentrations of Co (< 1 ppm), Ni (< 4 ppm) and V (< 6 ppm) in the GBC rocks (Table 1a) argue against their origin by extensive fractional crystallization of mantle-derived mafic magma. The GBC rocks plot in the A2 field (Fig. 7) in the discrimination diagrams of Eby (1992) suggesting that the rocks were probably generated by the melting of dehydrated crust. The SLG granites [E-lobe, AGS porphyry (Magyarosi 2022) and Winterland porphyry (Table 1b)] also plot into the A2 field.

Nd-depleted mantle model ages of GBC and SLG are Neoproterozoic (~ 800 to 1000 Ma) comparable with the age of the Avalonian basement rocks (Kerr et al. 1993b; Kellett et al. 2014). This suggests that the parent magma was generated by partial melting of anhydrous Neoproterozoic lower crust (Kerr et al. 1995). Such sources are also consistent with Sr isotopic ratios, although there is a limited amount of comparison data for the Devonian felsic rocks from this part of Newfoundland (Kerr et al. 1993a). The range of ε_{Nd} for the GBC and SLG is comparable to that of the Neoproterozoic Burin Group outcropping east of the SLG (Fig. 1b). The isotopic signature of mafic rocks of ~ 760 Ma old Burin Group (Fig. 11) is similar to that inferred for the source of the main phase of the Avalon magmatism (Murphy and Dostal 2007; Murphy et al. 2008a,b). In fact, Murphy et al. (2008a) argued that the Burin Group is representative of the geochemical and isotopic composition of the Avalonian basement, although the group itself cannot be the source, because its metamorphic grade is much too low. The chemical characteristics of the GBC and SLG, as well as other Devonian A-type granitic rocks of this part of the Avalonia, particularly their enrichment in some incompatible trace elements, imply that their source likely contained an admixture of metasomatized lithospheric mantle (e.g., Kellet et al.

Table 2 Sr and Nd isotopic composition of GBC and SLG rocks

Sample		Age (Ma)	Rb (ppm)	Sr (ppm)	$^{87}Rb/^{86}Sr$	$^{87}Sr/^{86}Sr_{(m)}$	2σ	$^{87}Sr/^{86}Sr_{(i)}$	Nd (ppm)	Sm (ppm)	$^{147}Sm/^{144}Nd$	$^{143}Nd/^{144}Nd_{(m)}$	2σ	$^{143}Nd/^{144}Nd_{(i)}$	$\varepsilon_{Nd}(t)$	T_{DM} (Ma)
.73–6	QF porphyry	377	209	44.3	13.7	0.777945	4	0.704168	34.5	8.59	0.1506	0.512662	7	0.512290	2.7	928
.74–3	QF porphyry	377	200	32.0	18.3	0.801983	8	0.704018	35.86	9.07	0.1529	0.512664	5	0.512287	2.6	956
.74–1	QF porphyry	377	212	29.7	20.9	0.816356	9	0.704315	44.2	10.80	0.1478	0.512642	8	0.512277	2.4	934
Kerr	QF porphyry	377							40.2	10.3	0.1499	0.512636		0.512266	2.2	978
Kerr	SLG granite	375							50.2	12.4	0.1450	0.512677		0.512321	3.2	823

$^{87}Sr/^{86}Sr_{(m)}$ and $^{143}Nd/^{144}Nd_{(m)}$ are measured values; $^{87}Sr/^{86}Sr_{(i)}$, $^{143}Nd/^{144}Nd_{(i)}$ and $\varepsilon_{Nd}(t)$ are age-corrected to 377 and 375 Ma, respectively

T_{DM} depleted mantle age calculated according to DePaolo (1988); *Kerr* data from Kerr et al. (1995), *QF porphyry* quartz–feldspar porphyry from GBC, *SLG granite* peralkaline granite from SLG intrusion

2014; Papoutsa et al. 2016; Murphy et al. 2008b). Felsic magmas such as those of the SLG and GBC are considered to reflect partial melting of the metasomatized lower crust followed by fractional crystallization during ascent of the melts. The enrichment of the source in incompatible elements, including F, Th, U, and REE through subduction and/or metasomatism considerably enhanced the concentrations of these elements in the melts. In the source, fluorine was probably stored in phlogopite/biotite and amphibole. The distinct negative Eu anomalies on the chondrite-normalized REE plots (Fig. 8) are due to feldspar fractionation. The weak fractionation of HREE likely reflects an absence of garnet in the source, supported an origin at relatively low pressure, at a depth that is shallower than the garnet stability field.

The primitive mantle-normalized plots of the GBC rocks with distinct negative Sr, Ba, and Eu anomalies (Fig. 9) suggest that the rocks underwent extensive fractional crystallization dominated by feldspars, whereas the negative Ti and P anomalies, respectively, reflect the fractionation of Fe-Ti oxide and apatite. The Rb/Sr vs Sr relationships (Fig. 10) imply that feldspar fractionation played a major role during GBC magma evolution.

The K/Rb ratios of granitic rocks can provide information on the role of fluids (e.g., Shaw 1968). The crustal average of K/Rb ratio is ~ 250 (Shaw 1968; Rudnick and Gao 2003). Shaw (1968) argued that K/Rb ratios < 150 result from extensive fluid-melt/rock interaction. Both the GBC and SLG have K/Rb values lower than the crust (Fig. 10), indicating the influence of fluids in their genesis (e.g., Shaw 1968; Dostal and Chatterjee 1995). However, the GBC rocks have higher K/Rb ratios (~ 190 to 220) than the SLG rocks (~ 80 to 160), implying that the hydrothermal alteration (including late magmatic and post-magmatic fluid interactions) affected the SLG rocks notably more than the GBC rocks. The hydrothermal alteration of the SLG might have accompanied fluorite mineralization during degassing (Magyarosi 2022).

Relation between the GBC and SLG and fluorite mineralization

The obtained age (~ 376 Ma) for the GBC is closely comparable to the age of the SLG, particularly the AGS, implying they were emplaced during the same magmatic episode. Comparison of major- and trace-element compositions of relatively unaltered samples from the SLG and GBC suites shows that the rocks are rather similar (Figs. 6 and 9). They are both highly fractionated leucocratic high-silica rocks with low contents of MgO but high alkalis and many incompatible trace elements, such as REE, Th, U, Rb, and Cs. Although ferroan (Frost et al. 2001), within-plate and A-types (Fig. 7) with similar

Table 3 Saturation temperatures of accessory minerals

	Zircon T_{Zr} (°C)					Monazite T_{Mz} (°C)			$T_{Ti\ in\text{-}zircon}$ (°C)		
	W&H (1983)			Boehnke et al. (2013)		Montel (1993)			Watson et al. (2006)		
	n	aver	st. dev	aver	st. dev	*n*	aver	st. dev	*n*	aver	st. dev
GBC	17	787	8	742	10	17	798	22	25	807	58
SLG	30	873	38	843	46	35	804	52			
AGS	2	779	4	731	6	2	769	4			

T_{Zr} zircon saturation temperature calculated according to Watson and Harrison (1983) (W&H), and Boehnke et al. (2013), T_{Mz} monazite saturation temperature calculated according to Montel (1993); $T_{Ti\ in\text{-}zircon}$ calculated according to Watson et al. (2006), *n* number of analyses, *aver* average, *st. dev.* standard deviation, *GBC* Grand Beach Complex (data from Table 1), *SLG* St. Lawrence Granite (data from Magyarosi 2022), AGS sills and dikes (data from Magyarosi 2022)

isotopic characteristics [($\varepsilon_{Nd}(t)$ Table 2], they differ in oxidation state and alkalinity. The GBC rocks are more oxidized than the SLG (Fig. 10a). The SLG have both A/CNK and A/NK ~ 1, whereas the GBC rocks are mildly peraluminous and plot into the peraluminous field on the conventional A/CNK versus A/NK diagram (Fig. 6b). The subtle differences in oxidation state and alkalinity cannot be readily explained by fractional crystallization but require an additional process likely crustal contamination. The role of crustal contamination is consistent with the slightly lower $\varepsilon_{Nd}(t)$ value of the GBC compared to the SLG granite (Table 2). Likewise, the GBC rocks have a more pronounced negative Nb anomaly on the primitive mantle-normalized plots, which suggests crustal involvement (Fig. 9). There are also subtle dissimilarities in saturation temperatures between these two suites. The SLG has higher zircon and monazite saturation temperatures relative to GBC (Table 3).

The SLG is a shallow-seated high temperature A-type granitic pluton (emplaced at depth of ~ 1 to 2 km, Magyarosi 2022) associated with the late magmatic hydrothermal fluorine-rich fluids, which produced fluorite mineralization as well as extensive alteration of the intrusion. Magyarosi (2022) argued that some of the mineralizing fluids, which resulted from devolatilization of the granitic magma, escaped into the surrounding rocks where they also generated fluorite mineralization. The close proximity of the SLG and the contemporaneous volcanic complex suggests that the GBC can host fluorite mineralization. The SLG and GBC show similarities to the NYF (Nb–Y–F) granites/pegmatites of Černý et al. (2005).

Tectonic settings

The Appalachian orogen was formed by the Paleozoic accretion of several distinct tectonic terranes (microcontinents, blocks, arcs, etc.) to the eastern margin of the Laurentia during the progressive closure of the Iapetus and Rheic oceans (e.g., van Staal et al. 2009). In Newfoundland, closure of Iapetus was completed by Late Silurian (at ~ 420 Ma). The last stage was characterized by accretion of the Avalonia microcontinent to Ganderia (an eastern part of Laurentia accreted during the Early Silurian). The juxtaposition of Avalonia against Ganderia (e.g., Schofield and D'Lemos 2000; van Staal et al. 2009) was accompanied by emplacement of voluminous plutonic suits of Silurian–Early Devonian age along the eastern boundary of Ganderia (e.g., Kellett et al. 2014). Subsequently, these rocks were intruded by undeformed Middle-to-Late Devonian (400–360 Ma) granitic plutons (Kellett et al. 2014) encompassing a variety of granitic compositions: S-, I-, and A-type granites (Fig. 11; van Staal et al 2009). In southeastern Newfoundland, these rocks form a curvilinear belt of post-tectonic granitic intrusions that occur along the boundary between Ganderia and Avalonia. The SLG and GBC are the part of this Devonian belt, which contains granitic intrusions with similar ages such as the Francois pluton (378 ± 2 Ma) and Ackley granite (377 ± 3 Ma) (Kerr et al. 1993a; Kellett et al. 2014). Some undeformed intrusions host rare metal mineralization (e.g., Kerr et al. 1993b; Kerr and McNicoll 2012). Kellett et al. (2014) noted that the reactivation of the Ganderia–Avalonia bounding faults lasted at least 30 Ma, from ~ 395 to ~ 365 Ma.

Granitic plutons of similar age also occur in Nova Scotia (e.g., Bickerton et al. 2022; Currie et al. 1998; Papoutsa et al. 2016; Dostal et al. 2004, 2006), suggesting that the emplacement of all these granitic bodies was a regional event. The origin of the Late Paleozoic felsic rocks in this part of the Appalachians is probably related to failed slab subduction with melting triggered by mantle upwelling through the slab breach (Fig. 12). Magmatism was post-tectonic and associate with extension, widespread uplift, and exhumation (Schofield and D'Lemos 2000; Kellet et al. 2014). Some Avalonian A-type felsic rocks in Newfoundland including the SLG and GBC were derived from lower crustal basement, which contained variable but minor amounts

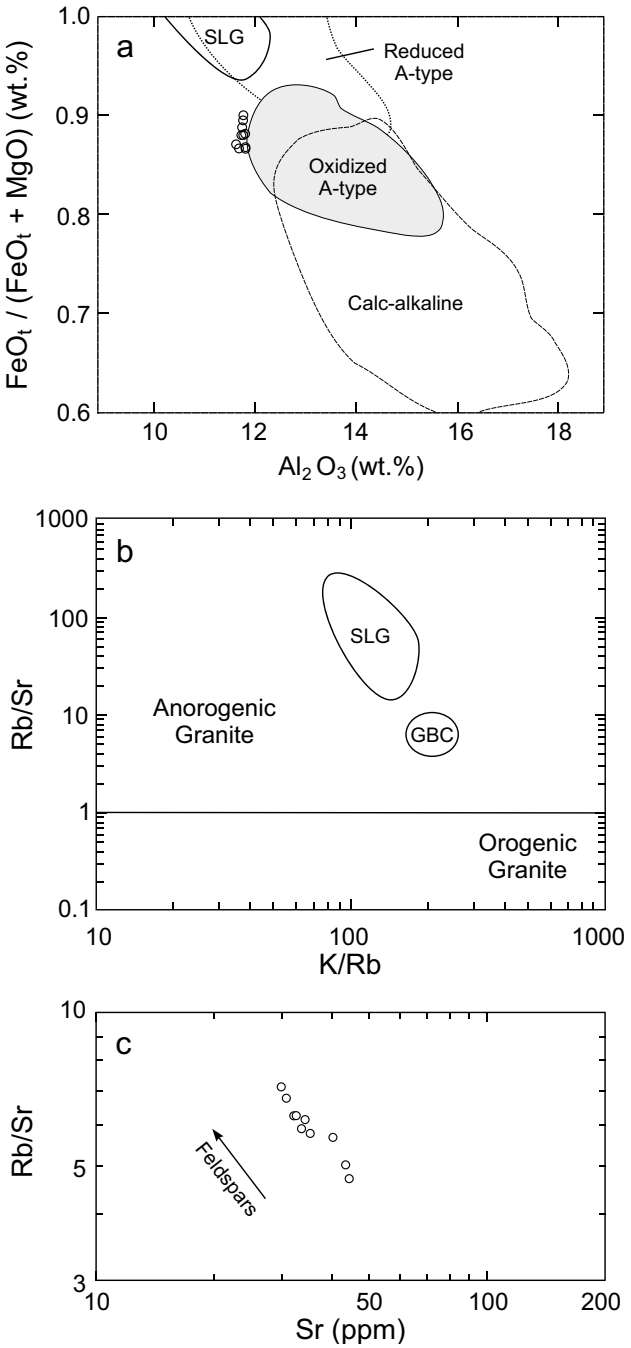

Fig. 10 **a** $FeO_t/(FeO_t+MgO)$ versus Al_2O_3 (wt.%) diagram for the fresh GBC rocks (circles) showing compositional fields of reduced and oxidized A-type granites and calc-alkaline granites after Dall'Agnol and Oliveira (2007). The solid curve outlines the field for SLG rocks (data from Magyarosi 2022). **b** Rb/Sr versus K/Rb plot for GBC and SLG rocks. The boundary (at Rb/Sr = 1) that separates the fields of orogenic and anorogenic granites is after Abdel-Rahman (2006). *GBC* field of fresh GBC rocks, *SLF* field of SLG rocks (data from Magyarosi 2022). **c** Rb/Sr versus Sr (ppm) diagram for the fresh GBC rocks (circles). The vector depicts the fractionation trends of the compositional changes in the residual liquid when feldspars are progressively removed from the magma during fractional crystallization

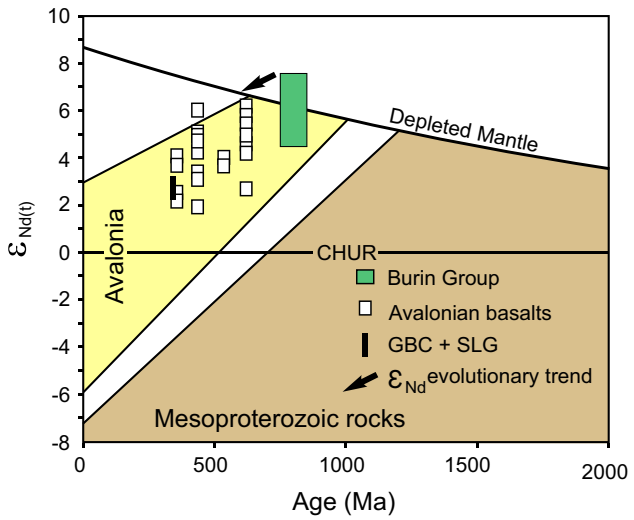

Fig. 11 $\varepsilon_{Nd}(t)$ versus time plot comparing Sm–Nd isotopic data of the SLG and GBC with basaltic rocks of Avalonia of the Canadian Maritimes (Murphy et al. 2011; Dostal et al. 2022). Shaded area (envelope) is the Avalonian basement and subcontinental lithospheric mantle (SCLM; after Keppie et al. 2012; Murphy et al. 2011; Dostal et al. 2022). The field for Mesoproterozoic rocks is from Murphy et al. (2008b). *CHUR* chondritic uniform reservoir

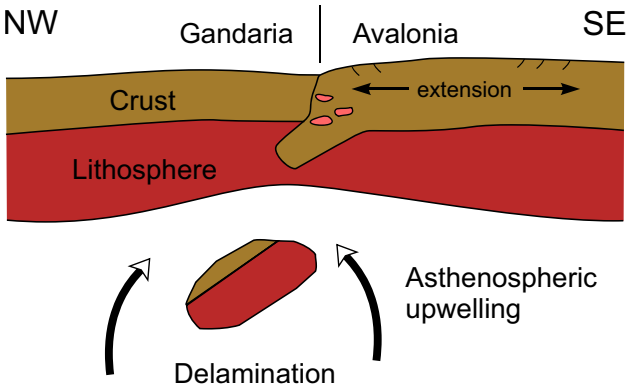

Fig. 12 Schematic diagram illustrating the tectono-magmatic evolution of the Avalonian Late Devonian felsic igneous rocks in southeastern Newfoundland highlighting the process of partial melting in the lower crust caused by the upwelling of mantle material through the slab breach due to slab failure and delamination. Not to scale

of metasomatized lithospheric mantle. Melting of such a source produced parental melts that fractionated to produce SLG and GBC (Fig. 12). A-type granites are common in the Paleozoic of Avalonia, because the crust was dehydrated in the late Neoproterozoic (e.g., Murphy et al. 2018). The Sm–Nd signature of the juvenile crust (Fig. 11) that melted to yield the A-type magmas in this part of the Avalonia may be derived from the source of the 760 Ma Burin Group (Murphy et al. 2008a).

Conclusions

The quartz porphyries of the Grand Beach volcanic complex have a composition characteristic of alkali rhyolites, high in silica but low in Mg, Fe, and Ca and have a low Mg/Fe ratio. They are weakly peraluminous A-type felsic rocks with high contents of incompatible trace elements, such as REE Th, U, and Rb. They have positive $\varepsilon_{Nd}(t)$ values (~ + 2.5) and their Nd-depleted mantle model ages (~ 0.9 Ga) are consistent with the derivation of parental magma of these rocks from metasomatized Avalonian lower crustal basement followed by fractional crystallization (Fig. 11). These highly fractionated rocks are compositionally similar to the rocks of the SLG. They are a part of the Devonian magmatic episode, which produced the SLG and several other granitic intrusions. In particular, the emplacement of the GBC coincides with the emplacement of mineralized AGS sills and dikes (in the central part of the pluton). Both AGS and GBC represent slightly earlier phases of the SLG and host fluorite mineralization. GBC probably represents a volcanic equivalent of SLG. The subtle compositional differences between the volcanic and plutonic rocks are likely the result of the interaction of the parental magma with crustal material and fluids (including late magmatic or post-magmatic fluids).

The results show that the spatially and temporally related felsic plutonic and volcanic rocks have a similar major- and trace-element characteristics and similar range of isotopic ratios. Both rock-types were formed by the same processes and derived from similar sources. The minor differences between these two types of rocks are related to the last stages of evolution and emplacement.

Supplementary Information The online version contains supplementary material available at https://doi.org/10.1007/s00531-023-02375-6.

Acknowledgements This research was supported by NSERC (Canada) Discovery grants to J. Dostal, CONACYT Grant #7351 to L. Solari and the National Natural Science Foundation of China (Grants Nos. 42130309 and 41972066) to C. Ma. The authors thank Carlos Ortega-Obregón for maintaining the LA-ICP-MS facilities at CGEO, UNAM and Randy Corney for technical assistance. Constructive reviews by Drs. John Greenough and Brendan Murphy improved the manuscript.

Funding The work of Luigi Solari was funded by Consejo Nacional de Ciencia y Tecnologia, under Grant #7351, and the work of Changqian Ma was funded National Natural Science Foundation of China, under Grant Nos. 42130309 and 41972066.

Data availability The authors declare that the data supporting the finding of this study are available within the paper.

Declarations

Conflict of interest The authors declare that they have no known competing financial interests or personal relationships that could have appeared to influence the work reported in this paper.

References

Abdel-Rahman AM (2006) Petrogenesis of anorogenic peralkaline granitic complexes from eastern Egypt. Mineral Mag 70:27–50

Ackerman L, Žák K, Skála R, Rejšek J, Křížová Š, Wimpenny J, Magna T (2020) Sr–Nd–Pb isotope systematics of Australasian tektites: Implications for the nature and composition of target materials and possible volatile loss of Pb. Geochim Cosmochim Acta 276:135–150

Annen C, Blundy JD, Leuthold J, Sparks RSJ (2015) Construction and evolution of igneous bodies: towards an integrated perspective of crustal magmatism. Lithos 230:206–221

Bachmann O, Miller CF, de Silva SL (2007) The volcanic-plutonic connection as a stage for understanding crustal magmatism. J Volcanol Geoth Res 167:1–23

Bau M (1996) Controls on the fractionation of isovalent trace elements in magmatic and aqueous systems: evidence from Y/Ho, Zr/Hf and lanthanide tetrad effect. Contrib Miner Petrol 123:323–333

Bell K, Blenkinsop J, Strong DF (1977) The geochronology of some granitic bodies from eastern Newfoundland and its bearing on Appalachian evolution. Can J Earth Sci 14:456–476

Bickerton L, Kontak DJ, Murphy JB, Kellett DA, Samson IM, Marsh JH, Dunning G, Stern R (2022) The age and origin of the South Mountain Batholith (Nova Scotia, Canada) as constrained by zircon U–Pb geochronology, geochemistry, and O–Hf isotopes. Can J Earth Sci. https://doi.org/10.1139/cjes-2021-0097

Boehnke P, Watson EB, Trail D, Harrison TM, Schmitt AK (2013) Zircon saturation re-revisited. Chem Geol 351:324–334

Bonin B (2007) A-type granites and related rocks: evolution of a concept, problems and prospects. Lithos 97:1–29

Boynton WV (1984) Cosmochemistry of the rare earth elements; meteorite studies. In: Henderson P (ed) Rare earth element geochemistry. Elsevier, Amsterdam, The Netherlands, pp 63–114

Černý P, Blevin PL, Cuney M, London D (2005) Granite-related ore deposits. 100th anniversary volume. Society of Economic Geologists, pp 337–370

Cheng Y, Spandler C, Chang Z, Clarke G (2018) Volcanic–plutonic connections and metal fertility of highly evolved magma systems: a case study from the Herberton Sn–W–Mo Mineral Field, Queensland, Australia. Earth Planet Sci Lett 486:84–93

Currie KL, Whalen JB, Davis WJ, Longstaffe FJ, Cousens BL (1998) Geochemical evolution of peraluminous plutons in southern Nova Scotia, Canada-a pegmatite-poor suite. Lithos 44:117–140

Dall Agnol R, Oliviera DC (2007) Oxidized, magnetite-series, rapakivi-type granites pf Carajas, Brazil: implications for classification and petrogenesis of A-type granites. Lithos 93:215–233

De la Roche H, Leterrier J, Grandclaude P, Marchal M (1980) A classification of volcanic and plutonic rocks using R_1R_2-diagram and major-element analyses - Its relationships with current nomenclature. Chem Geol 29:183–210

DePaolo DJ (1988) Neodymium isotope geochemistry: an introduction. Springer, New York, p 187

Dostal J, Chatterjee AK (1995) Origin of topaz-bearing and related peraluminous granite of the Late Devonian Davis Lake Pluton, Nova Scotia, Canada: crystal versus fluid fractionation. Chem Geol 123:67–88

Dostal J, Shellnutt JG (2016) Origin of peralkaline granites of the Jurassic Bokan Mountain complex (southeastern Alaska) hosting rare metal mineralization. Int Geol Rev 58:1–13

Dostal J, Chatterjee AK, Kontak DJ (2004) Chemical and isotopic (Pb, Sr) zonation in a peraluminous granite pluton: role of fluid fractionation. Contrib Miner Petrol 147:74–90

Dostal J, Keppie JD, Jutras P, Miller BV, Murphy JB (2006) Evidence for the granulite-granite connection: penecontemporaneous

high-grade metamorphism, granite magmatism and core complex development in the Liscomb Complex, Nova Scotia, Canada. Lithos 86:77–90

Dostal J, Kontak DJ, Karl SM (2014) The early Jurassic Bokan Mountain peralkaline granitic complex (southeastern Alaska): geochemistry, petrogenesis and rare-metal mineralization. Lithos 202–203:395–412

Dostal J, Corney R, Church BN, Connolly RM (2021) Petrogenesis of Eocene shoshonitic rocks from South-Central British Columbia. Lithos 398–399:106289

Dostal J, Jutras P, Wilson RA (2022) Geochemical and Nd isotopic constraints on the origin of the uppermost Silurian rhyolitic rocks in the northern Appalachians (northern New Brunswick): tectonic implications. In: Kupier YD, Murphy JB, Nance RD, Strachan RA, Thompson MD (eds) New developments in the Appalachian-Caledonian-Variscan Orogen, vol 554. Geological Society of America Special Paper, pp 121–122

Eby N (1992) Chemical subdivision of the A-type granitoids: Petrogenetic and tectonic implications. Geology 20:641–644

Frost BR, Barnes CG, Collision WJ, Arculus RJ, Ellis DJ, Frost CD (2001) A geochemical classification for granitic rocks. J Petrol 42:2033–2048

Harris NBW, Pearce JA, Tindle AG (1986) Geochemical characteristics of collision zone magmatism. Geol Soc Spec Pub 99:67–81

Hibbard JP, van Staal CR, Rankin DW, Williams H (2006) Lithotectonic map of the Appalachian Orogen, Canada–United States of America. Geological Survey of Canada, Map 2096A, scale 1:1 500 000

Irber W (1999) The lanthanide tetrad effect and its correlation with K/Rb, Eu/Eu*, Sr/Eu, Y/Ho and Zr/Hf of evolving peraluminous granite suites. Geochim Cosmochim Acta 63:489–508

Jutras P, Dostal J (2019) The Upper Visean Magdalen Islands basalts of Eastern Quebec, Canada. J Geol 127:505–526

Kellett DA, Rogers N, McNicoll V, Kerr A, van Staal C (2014) New age data refine extent and duration of Paleozoic and Neoproterozoic plutonism at Ganderia-Avalonia boundary, Newfoundland. Can J Earth Sci 51:943–972

Keppie JD, Murphy JB, Nance RD, Dostal J (2012) Mesoproterozoic Oaxaquia-type basement in peri-Gondwanan terranes of Mexico, the Appalachians and Europe: TDM age constraints on extent and significance. Int Geol Rev 54:313–324

Kerr A, McNicoll V (2012) New U–Pb geochronological constraints from mineralized granites in southern Newfoundland. In: Current Research. Government of Newfoundland and Labrador, Department of Natural Resources, Geological Survey, Report 121, pp 21–38

Kerr A, Dunning GR, Tucker RD (1993a) The youngest Paleozoic plutonism of the Newfoundland Appalachians: U-Pb ages from the St. Lawrence and François granites. Can J Earth Sci 30:2328–2333

Kerr A, Dickson WL, Hayes JP, Fryer BJ (1993b) Devonian post-orogenic granites on the southeast margin of the Newfoundland Appalachians: a review of geology, geochemistry, petrogenesis and mineral potential. In: Current Research, Newfoundland Department of Natural Resources, Geological Survey, Report 93–1. p. 239–279

Kerr A, Jenner GA, Fryer BJ (1995) Sm–Nd isotopic geochemistry of Precambrian to Paleozoic granitoid suites and the deep-crustal structure of the southeast margin of the Newfoundland Appalachians. Can J Earth Sci 32:224–245

Krogh TE, Strong DF, O'Brien SJ, Papezik VS (1988) Precise U-Pb zircon dates from the Avalon Terrane in Newfoundland. Can J Earth Sci 148:115–136

La Flèche MR, Camire G, Jenner GA (1998) Geochemistry of post-Acadian, Carboniferous continental intraplate basalts from the Maritimes Basin, Magdalen Islands, Quebec, Canada. Chem Geol 148:115–136

Li Z, Wang XC, Wilde SA, Liu L, Li WX, Yang XM (2018) Role of deep-water cycling in the growth and evolution of continental crust: constraints from Cretaceous magmatism in southeast China. Lithos 302:126–141

Liu YS, Gao S, Hu ZC, Gao CG, Zong KQ, Wang DB (2010) Continental and oceanic crust recycling-induced melt-peridotite interactions in the Trans-North China Orogen: U-Pb dating, Hf isotopes and trace elements in zircons of mantle xenoliths. J Petrol 51:537–571

Loucks RR, Fiorentini ML, Henriquez GJ (2020) New magmatic oxybarometer using trace elements in zircon. J Petrol 61:3

Lundstrom CC, Glazner AF (2016) Silicic magmatism and the volcanic-plutonic connection. Elements 12:91–96

Magyarosi Z (2022) Late-magmatic processes in the St. Lawrence granite: implications for fluorite mineralization. J Geochem Explor 239:107014

Magyarosi Z, Sparkes BA, Conliffe J, Dunning GR (2019) The AGS fluorite deposit, St. Lawrence: paragenetic sequence, fluid inclusion analysis, structural control, host rock geochronology and implications for ore genesis. In: Current Research. Government of Newfoundland and Labrador, Department of Natural Resources, Geological Survey, Report 19-1, pp 59–83

McDonough WF, Sun SS (1995) The composition of the Earth. Chem Geol 120:229–253

Miller CF, McDowell SM, Mapes RW (2003) Hot and cold granites? Implications of zircon saturation temperatures and preservation of inheritance. Geology 31:529–532

Mills A, Dunning GR, Sandeman HA (2021) Lithogeochemical, isotopic, and U-Pb (zircon) age constraints on arc to rift magmatism, northwestern and central Avalon Terrane, Newfoundland, Canada: implications for local lithostratigraphy. Can J Earth Sci 58:332–354

Monecke T, Kempe U, Monecke J, Sala M, Wolf D (2002) Tetrad effect in rare earth element distribution patterns: a method of quantification with application to rock and mineral samples from granite-related rare metal deposits. Geochim Cosmochim Acta 66:1185–1196

Montel JM (1993) A model for monazite/melt equilibrium and application to the generation of granitic magmas. Chem Geol 110:127–146

Murphy JB, Dostal J (2007) Continental mafic magmatism of different ages in the same terrane: constraints on the evolution of an enriched mantle source. Geology 35:335–338

Murphy JB, McCausland PJA, O'Brien SJ, Pisarevsky S, Hamilton MA (2008a) Age, geochemistry and Sm–Nd isotopic signature of the 0.76 Ga Burin Group: Compositional equivalent of Avalon basement? Precambr Res 165:37–48

Murphy JB, Dostal J, Keppie JD (2008b) Neoproterozoic-Early Devonian magmatism in the Antigonish Highlands, Avalon terrane, Nova Scotia: tracking the evolution of the mantle and crustal sources during the evolution of the Rheic Ocean. Tectonophysics 461:181–201

Murphy JB, Dostal J, Gutierrez-Alonso G, Keppie JD (2011) Early Jurassic magmatism on the northern margin of CAMP: derivation from a Proterozoic sub-continental lithospheric mantle. Lithos 123:158–164

Murphy JB, Shellnutt JG, Collins WJ (2018) Late Neoproterozoic to Carboniferous genesis of A-type magmas in Avalonia of northern Nova Scotia: repeated partial melting of anhydrous lower crust in contrasting tectonic environments. Int J Earth Sci 107:587–599

O'Brien SJ, Strong DF, Strong P, Taylor SW, Wilton DH (1976) Geology of the Marystown–St. Lawrence area. In: Report of Activities, 1975. Government of Newfoundland and Labrador, Department of Mines and Energy, Mineral Development Division, Report 76-1

O'Brien SJ, Strong PG, Evans JL (1977) The geology of the Grand Bank (1M/4) and Lamaline (1L/3) Map Areas, Burin Peninsula,

Newfoundland. Government of Newfoundland and Labrador, Department of Mines and Energy, Mineral Development Division. Report 77-7, p 16

O'Brien SJ, O'Brien BH, Dunning GR, Tucker RD (1996) Late Neoproterozoic Avalonian and related peri-Gondwanan rocks of the Newfoundland Appalachians. Special Paper 304: Avalonian and related peri-Gondwanan terranes of the Circum-North Atlantic. Geological Society of America, pp 9–28

Papoutsa A, Pe-Piper G, Piper DJW (2016) Systematic mineralogical diversity in A-type granitic intrusions: control on magmatic source and geological processes. Geol Soc Am Bull 128:487–501

Paton C, Woodhead JD, Hellstrom JC, Hergt JM, Greig A, Maas R (2010) Improved laser ablation U-Pb zircon geochronology through robust downhole fractionation correction. Geochem, Geophys, Geosyst 11(3):6

Pearce JA (1996) A user's guide to basalt discrimination diagrams. In: Wyman DA (ed) Trace element geochemistry of volcanic rocks: applications for massive sulphide exploration, vol 12. Geological Association of Canada, NF, pp 79–113

Pe-Piper G, Piper DJW (1998) Geochemical evolution of Devonian-Carboniferous igneous rocks of the Magdalen basin, Eastern Canada: Pb and Nd isotope evidence for mantle and lower crustal sources. Can J Earth Sci 35:201–221

Petrus JA, Kamber BS (2012) VizualAge: a novel approach to laser ablation ICP-MS U-Pb geochronology data reduction. Geostand Geoanal Res 36:247–270

Rudnick RL, Gao S (2003) Composition of the continental crust. In: Holland HD, Turekian KK (eds) Treatise on geochemistry, the crust, vol 3. Elsevier-Pergamon, Oxford, pp 1–64

Schofield DI, D'Lemos RS (2000) Granite petrogenesis in the Gander Zone, NE Newfoundland: mixing of melts from multiple sources and the role of lithospheric delamination. Can J Earth Sci 37:535–547

Shaw DM (1968) A review of K-Rb fractionation trends by covariance analyses. Geochim Cosmochim Acta 32:573–601

Shaw DM, Dostal J, Keays RR (1976) Additional estimates of continental surface Precambrian shield composition in Canada. Geochim Cosmochim Acta 40:73–83

Sláma J et al (2008) Plešovice zircon- new natural reference material for U–Pb and Hf isotopic microanalysis. Chem Geol 249:1–35

Solari L, Torres de León R, Hernández Pineda G, Sole J, Solis-Pichardo G, Hernández-Trevino T (2007) Tectonic significance of Cretaceous Tertiary magmatic and structural evolution of the northern margin of the Xolapa Complex, Tierra Colorada area, southern Mexico. Bull Geol Soc Am 119:1265–1279

Solari L, González-León CM, Ortega-Obregón C, Valencia-Moreno M, Rascón-Heimpel MA (2018) The Proterozoic of NW Mexico revisited; U–Pb geochronology and Hf isotopes of Sonoran rocks and their tectonic implications. Int J Earth Sci 107:845–861

Strong DF, O'Brien SJ, Strong PG, Taylor SW, Wilton DH (1976) Geology of the St. Lawrence and Marystown Map Sheets (1L/14, 1M/3), Newfoundland, Preliminary Report for Open File Release, NFLD/895, pp 44

Strong DF, O'Brien SJ, Taylor SW, Strong PG, Wilton DH (1978) Geology of the Marystown (1M/13) and St. Lawrence (1L/14) Map Areas, Newfoundland. Government of Newfoundland and Labrador, Department of Mines and Energy. Mineral Development Division, Report 78-7, pp 81

Strong DF, Fryer BJ, Kerrich R (1984) Genesis of the St. Lawrence fluorspar deposits as indicated by fluid inclusion, rare earth element, and isotopic data. Econ Geol 79:1142–1158

Sun SS, McDonough WF (1989) Chemical and isotopic systematics of oceanic basalts: implications for mantle composition and processes. Geol Soc Lond Spec Publ 42:313–345

Sylvester PJ (1989) Post-collisional alkaline granites. J Geol 97:261–280

Teng HC, Strong DF (1976) Geology and geochemistry of the St. Lawrence peralkaline granite and associated fluorite deposits, Southeast Newfoundland. Can J Earth Sci 13:1374–1385

Trail D, Watson EB, Tailby ND (2012) Ce and Eu anomalies in zircon as proxies for the oxidation state of magmas. Geochim Cosmochim Acta 97:70–87

van Staal CR, Whalen JB, Valverde-Vaquero P, Zagorevski A, Rogers N (2009) Pre-Carboniferous, episodic accretion-related, orogenesis along the Laurentian margin of the northern Appalachians. Geol Soc Lond Spec Publ 327:271–316

Vermeesch P (2018) Isoplot R: a free and open toolbox for geochronology. Geosci Front 9:1479–1493

Wang F, Liu SA, Li S, He Y (2013) Contrasting zircon Hf–O isotopes and trace elements between ore-bearing and ore-barren adakitic rocks in central-eastern China: implication for genetic relation to Cu–Au mineralization. Lithos 156:97–111

Watson EB, Harrison TM (1983) Zircon saturation revisited: temperature and composition effects in a variety of crustal magma types. Earth Planet Sci Lett 64:295–304

Watson EB, Wark DA, Thomas JB (2006) Crystallization thermometers for zircon and rutile. Contrib Miner Petrol 115:413–433

Whalen JB, Currie KL, Chappell BW (1987) A-type granites: geochemical characteristics, discrimination and petrogenesis. Contrib Miner Petrol 95:407–419

Whalen JB, Jenner GA, Hegner E, Gariepy C, Longstaffe FJ (1994) Geochemical and isotopic (Nd, O, and Pb) constraints on granite sources in the Humber and Dunnage zones, Gaspesie, Quebec, and New Brunswick: implications for tectonics and crustal structure. Can J Earth Sci 31:323–340

Whalen JB, Jenner GA, Longstaffe FJ, Hegner E (1996) Nature and evolution of the eastern margin of lapetus: geochemical and isotopic constraints from Siluro-Devonian granitoid plutons in the New Brunswick Appalachians. Can J Earth Sci 33:140–155

Whalen JB, McNicoll VJ, van Staal CR, Lissenberg CJ, Longstaffe FJ, Jenner GA, van Breemen O (2006) Spatial, temporal and geochemical characteristics of Silurian collision zone magmatism, Newfoundland Appalachians: an example of a rapidly evolving magmatic system related to slab break-off. Lithos 89:377–404

Wiedenberck M, Alle P, Corfu F, Griffin W, Meier M, Oberli F, Von Quadt A, Roddick JC, Spiegel W (1995) Three natural zircon standards for U–Th–Pb, Lu–Hf, trace element and REE analyses. Geostand Geoanal Res 19:1–23

Williams H (1984) Miogeoclines and suspected terranes of the Caledonian-Appalachian Orogen: tectonic patterns in the north Atlantic region. Can J Earth Sci 21:887–901

Winter JD (2001) An introduction to igneous and metamorphic petrology. Prentice Hall Inc, NJ, USA, p 606

Wu FY, Jahn BM, Wilde SA, Lo CH, Yui TF, Lin Q, Sun DY (2003) Highly fractionated I-type granites in NE China (I): geochronology and petrogenesis. Lithos 66:241–273

Zhu YX, Wang LX, Ma CQ, Wiedenbeck M, Wang W (2020) The Neoproterozoic alkaline rocks from Fangcheng area, East Qinling (China) and their implications for regional Nb mineralization and tectonic evolution. Precambr Res 350:105852